Diffraction from twisted nanowires: helicity revealed by anisotropy

Marc Gailhanou, Jean-Marc Roussel

JOURNAL OF APPLIED CRYSTALLOGRAPHY

ISSN 1600-5767

Diffraction from twisted nanowires: helicity revealed by anisotropy

Marc Gailhanou* and Jean-Marc Roussel

Aix-Marseille Université, CNRS, IM2NP, Marseille, France. *Correspondence e-mail: marc.gailhanou@univ-amu.fr

Received 1 August 2018
Accepted 21 September 2018

Edited by V. Holý, Charles University, Prague, Czech Republic

Keywords: simulated X-ray diffraction; torsion; twisted nanowires; helicity; anisotropy.

Supporting information: this article has supporting information at journals.iucr.org/j

The helical nature of twisted nanowires is studied by simulated X-ray diffraction. It is shown that this helicity is revealed by the anisotropy, which can be both an elastic anisotropy, through the warping displacement generated by torsion, or a shape anisotropy of the cross section. To support the analytical calculations, based on the kinematic theory of diffraction by helices, atomistic simulations of copper nanowires are performed.

1. Introduction

Diffraction from helices has a long history that dates back to the early 1950s and the understanding of the helical atomic structures of some of the most fundamental organic molecules or biomolecular compounds (Lucas & Lambin, 2005). The helix is indeed a very common structural feature in proteins (Pauling *et al.*, 1951; Barlow & Thornton, 1988), in DNA (Watson & Crick, 1953; Franklin & Gosling, 1953; Wilkins *et al.*, 1953) and in viruses such as the tobacco mosaic virus (Franklin, 1956; Caspar, 1956). The theory of diffraction from helical structures published by Cochran, Crick and Vand (CCV theory; Cochran *et al.*, 1952) has played a central role in the interpretation of diffraction from these organic structures. More recently, it has been applied to other assemblies of atomic helices such as inorganic carbon nanotubes (Lambin & Lucas, 1997) and imogolite nanotubes (Amara, 2014).

Interestingly, atomic helices can also be found in nanowires, which are our concern in the present work. In the field of the mechanics of nanowires, the fundamental problem of torsion can be viewed as the transformation of an assembly of straight atomic columns to an assembly of atomic helices, as shown in Fig. 1. Moreover, when they are monocrystalline and metallic, these nanowires can be twisted elastically up to very high torsion values with an elastic limit that increases when the nanowire radius decreases (Weinberger & Cai, 2010). This latter property, combined with the fact that X-ray diffraction is one of the most precise techniques for studying the state of strain in such small objects, led us to study the diffraction from twisted monocrystalline nanowires within the framework of the kinematic theory of diffraction by helices. Furthermore, as it is now possible, using X-rays and since the advent of third-generation synchrotron sources, to study single nanowires (Favre-Nicolin *et al.*, 2010; Labat *et al.*, 2015; Davtyan *et al.*, 2017), this publication is focused on diffraction from a single object.

As will be shown in this work, the high compacity and the symmetry of a metallic nanowire play a key role in its diffraction properties. Indeed, by contrast with helical structures such as DNA, the number of co-axial equivalent helices (*i.e.* having the same pitch and close radii) is very large in a

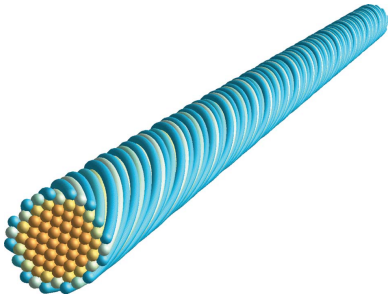

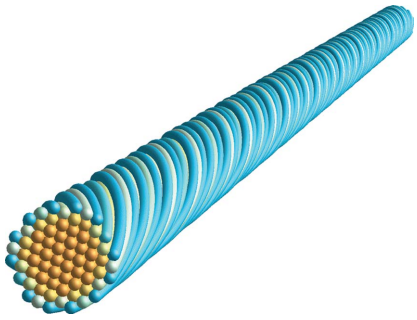

Figure 1
Perspective view of a twisted 1 nm radius ⟨011⟩ Cu nanowire with a torsion of 8×10^{-2} rad nm^{-1} and relaxed by MS simulation. For high values of the torsion α, the initial straight atomic columns become helices with a pitch $P = 2\pi/\alpha$ that may be lower or much lower than the coherence length of X-ray instruments.

twisted nanowire. Because of this large number, the symmetry tends to extinguish the helix diffraction orders that form the famous X-shaped diffraction pattern (sometimes named St Andrew's cross) specific to helicoidal structures. On the other hand, as soon as the symmetry is lowered in the plane of the cross section, we can expect the formation of X-shaped patterns in the reciprocal-space maps.

In the present work we examine two causes of symmetry lowering. The first concerns the anisotropy of the elastic constants that play a role in the torsion problem of a nanowire. It is well known that, depending on these elastic properties and the wire orientation, the torsion may induce a warping displacement along the wire axis of the atomic helices. The second is purely geometric and appears when the shape of the cross section is not circular but, for example, elliptic or hexagonal (shape anisotropy).

The paper is organized as follows. In §2 we recall the expressions of the torsion-induced warping displacement given by the theory of linear elasticity for ⟨001⟩ and ⟨011⟩ face-centred cubic (f.c.c.) nanowires with a circular or elliptic cross section. The displacement fields are compared with that obtained using atomistic molecular statics simulations on Cu nanowires, which will be used as model systems in this study. In §3 the basis of a twisted nanowire diffraction theory is given. First, the diffraction from a single twisted atomic column is derived within the framework of the kinematic theory. Then, the diffraction from a set of regularly spaced equivalent helices is detailed to highlight the extinction rule induced by this symmetry. In §4 the main results are given. We first investigate the effect of elastic anisotropy on diffraction through the warping displacement, and then the effect of shape anisotropy is presented. Finally, in §4.3 we discuss how these results apply to very small radius nanowires, how they may combine and how another kind of helicity appears when the nanowire contains an axial screw dislocation.

2. Elastic torsion warp

Torsion is, with traction and bending, one of the fundamental mechanical experiments that can be achieved on a particular object. The elasticity problem of the torsion of prismatic bars has excited the interest of numerous physicists, mathematicians and mechanicians since the 18th century (Higgins, 1942). Saint-Venant gave major contributions, including the prediction of the torsion warp, and his name, to this problem.

If the effects of surface stress are excluded, the solution to the elasticity equations (equilibrium equations, boundary conditions) can be obtained using the continuum elasticity theory of the generalized torsion of anisotropic homogeneous bars, as explained for example in the book by Lekhnitskii (1981). In the case of a low-symmetry nanowire orientation to which a torsion moment is applied, there are elastic displacements in addition to the geometric torsion displacements. Along the nanowire axis there is a warping displacement u_z, and in the nanowire cross section there is a displacement corresponding to a bending of the nanowire. It is, however, very common for the nanowire orientation to be along a low-indices direction and it can be considered as an orthotropic bar. We will restrict our study to such cases, and also to elliptic cross sections. In this case the bending displacement is equal to zero and the expression of the torsion-induced warping displacement is well established. In the case of cubic ⟨001⟩-oriented nanowires and in the reference frame attached to the three ⟨001⟩ directions, the warping displacement depends only on the elliptic cross-section anisotropy,

$$u_z^{\langle 001\rangle}(r,\theta) = \frac{\alpha}{2}\,\frac{a^2-b^2}{a^2+b^2}\,r^2\sin 2\theta, \qquad (1)$$

where (r, θ, z) are the cylindrical coordinates with respect to the crystallographic axes {[100], [010], [001]}. α is the torsion angle per unit length. The ellipse semi-axes, of lengths a and b, are aligned with the [100] and [010] directions, respectively.

For the common ⟨110⟩ f.c.c. metal nanowire orientation (Maurer *et al.*, 2007), the warping displacement depends on both shape anisotropy and elastic anisotropy,

$$u_z^{\langle 011\rangle}(r,\theta) = \frac{\alpha}{2}\,\frac{a^2-b^2A_z}{a^2+b^2A_z}\,r^2\sin 2\theta. \qquad (2)$$

Here, (r, θ, z) are the cylindrical coordinates with respect to the crystallographic axes $\{[100], [01\bar{1}], [011]\}$ and $A_z = 2C_{44}/(C_{11} - C_{12})$ is the usual Zener ratio which quantifies the elastic anisotropy in cubic crystals from the elastic stiffnesses C_{ij} given in the reference frame attached to the three ⟨100⟩ directions. A_z is greater than or equal to 1, the value of 1 corresponding to an elastic isotropic crystal. Although the A_z ratio is not universal (Ranganathan & Ostoja-Starzewski, 2008), its expression is simple and it is conveniently used in this expression of the torsion warping function. A variable elastic anisotropy will be obtained by considering metals with a Zener ratio ranging from values close to 1 to more than 3.

Equation (2) shows that, by choosing an a/b ratio equal to $(A_z)^{1/2}$, it is in principle possible to cancel the warping displacement. In the case of an isotropic material this is achieved with a circular cross section. To assess the validity of equation (2), we have performed molecular statics (MS) simulations on Cu nanowires presenting different cross

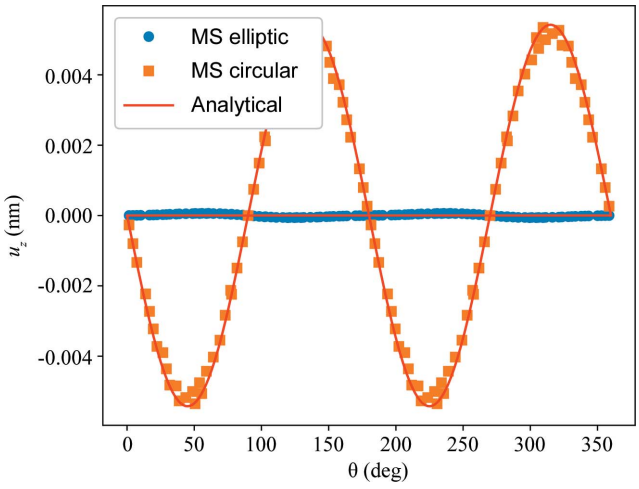

Figure 2
Torsion warp as a function of azimuth angle θ for atoms located at a radial distance r = 5 nm in the cases of a circular cross section and an elliptic cross section where $a/b = (A_z)^{1/2}$. MS simulations are represented with symbols and the analytical calculations using equation (2) with continuous lines. The nanowire is a Cu ⟨011⟩ nanowire, with either a circular cross section of radius 10 nm or an elliptic cross section with a = 13.5 nm and b = 7.4 nm so that $a/b = (A_z)^{1/2}$. The torsion is equal to 8×10^{-4} rad nm^{-1}.

sections. Interactions between copper atoms are modelled using a tight binding potential. Details of the simulations are given by Gailhanou & Roussel (2013). Fig. 2 shows the u_z displacement obtained from the MS simulations for atoms located at a radial distance $r = 5 \pm 0.15$ nm in Cu ⟨011⟩ having either a circular cross section or an elliptic cross section where $a/b = (A_z)^{1/2}$ and for which u_z is expected to be null. As also shown in previous work [Fig. 9*b* of Gailhanou & Roussel (2013)], both the prediction of the elasticity theory given by equation (2) and the atomistic simulations converge to the same warping displacement induced by the torsion.

3. Basis of a twisted nanowire diffraction theory

If we consider a cubic crystal nanowire oriented along an [*hkl*] direction, the only reflections that can be observed when the nanowire is twisted and when several twist periods are diffracting are the (nh, nk, nl) reflections, where n is an integer. In other directions the periodicity is lost because of the twist, and the untwisted nanowire diffraction spots become diffuse rings. Measuring these rings might be challenging owing to their very low intensity, especially for small-radius nanowires, and their broad distribution in reciprocal space. For this reason we focus here on the axial reflections.

The electronic density of a twisted nanowire can be written as the sum of the densities of the atomic columns j which are parallel to the nanowire axis without torsion and become helices when the nanowire is twisted,

$$\rho(\mathbf{r}) = \sum_j \rho_j(\mathbf{r}). \tag{3}$$

It is assumed that, because of the small nanowire transverse cross section, multiple scattering and absorption can be neglected. Within the kinematic approximation, the diffracted amplitude from this set of helices can be written as the sum of the amplitudes $\mathcal{A}_j$ scattered by each helix j of radius r_j,

$$\begin{aligned}\mathcal{A}(\mathbf{q}) &= f_e \sum_j \int \rho_j(\mathbf{r}) \exp(-i\mathbf{q}\cdot\mathbf{r})\, d\mathbf{r} \\ &= \sum_j \mathcal{A}_j(\mathbf{q}).\end{aligned} \tag{4}$$

Here, f_e is the classical electron scattering factor equal to $r_e\mathcal{P}$, r_e being the classical electron radius and $\mathcal{P}$ the polarization factor. All the helices have a period of $P = 2\pi/\alpha$, α being the torsion. The nanowire, of length L, is considered to be illuminated by a coherent uniform beam.

3.1. Diffraction from a single twisted atomic column

The calculation of the amplitude diffracted from a single helix given below corresponds to the CCV theory. It is also close to the calculations laid out by Lucas & Lambin (2005) and Prodanovic *et al.* (2016). We use cylindrical coordinates (r, φ, z) where the z axis coincides with the nanowire axis and where the origin of the frame is fixed at a distance $L/2$ from both nanowire ends. The electronic density of the helix of index j can be written as

$$\rho_j(\mathbf{r}) = \rho_j^{\text{at}}(\mathbf{r}) * \left[f_H(\mathbf{r})\, f_C(\mathbf{r})\, f_L(\mathbf{r})\right], \tag{5}$$

where

$$f_H(\mathbf{r}) = \delta(r - r_j)\frac{1}{r}\delta\left(\varphi - \varphi_0^j - \frac{2\pi z}{P}\right), \tag{6}$$

$$f_C(\mathbf{r}) = \sum_{m=-\infty}^{+\infty} \delta\left[z - (u_z^j + mP_a)\right], \tag{7}$$

$$f_L(\mathbf{r}) = \text{rect}(z/L). \tag{8}$$

Here, the symbol * is used for the convolution product and δ is the Dirac delta function. r_j and φ_0^j are, respectively, the radius and the azimuth of the helix j at $z = 0$. m is an integer, u_z^j is the z component of the helix displacement and P_a is the distance between atoms along the z direction. The amplitude $\mathcal{A}_j(\mathbf{q})$ diffracted by the helix j may thus be calculated from the product or convolution product of four Fourier transforms. The first is the atomic electron-density Fourier transform which is the atomic scattering factor considered here as isotropic:

$$f_j(q) = \int \rho_j^{\text{at}}(\mathbf{r}) \exp(-i\mathbf{q}\cdot\mathbf{r})\, d\mathbf{r}. \tag{9}$$

Let F_H, F_C and F_L be the Fourier transforms of, respectively, f_H the helix function, f_C the Dirac comb corresponding to the crystal lattice periodic positions and f_L the rectangle function related to the nanowire length. The helix Fourier transform F_H can be calculated using the cylindrical-coordinate Fourier transform (Diaz *et al.*, 2010) and the other two are thus also written using the cylindrical reciprocal coordinates (q_r, ψ_q, q_z) of the vector $\mathbf{q}$:

$$F_{\rm H}(\mathbf{q}) = 2\pi \sum_{n=-\infty}^{+\infty} J_n(q_r r_j) \exp\left[-in(\psi_q - \varphi_0^j + \pi/2)\right] \times \delta\left(q_z - n\frac{2\pi}{P}\right), \quad (10)$$

$$F_{\rm C}(\mathbf{q}) = \delta(q_r)\frac{1}{q_r}\delta(\psi_q)\frac{(2\pi)^3}{P_{\rm a}}\sum_{m=-\infty}^{+\infty}\exp\left(-im\frac{2\pi}{P_{\rm a}}u_z^j\right)\delta\left(q_z - m\frac{2\pi}{P_{\rm a}}\right), \quad (11)$$

$$F_L(\mathbf{q}) = (2\pi)^2\delta(q_r)\frac{1}{q_r}\delta(\psi_q)\; L\;\mathrm{sinc}\left(\frac{Lq_z}{2\pi}\right). \quad (12)$$

$\mathcal{A}_j(\mathbf{q})$ is obtained by combining these four Fourier transforms,

$$\mathcal{A}_j(\mathbf{q}) = \frac{f_{\rm e}}{(2\pi)^6} f_j(q)\left[F_{\rm H}(\mathbf{q}) * F_{\rm C}(\mathbf{q}) * F_L(\mathbf{q})\right] = \frac{f_{\rm e}L}{P_{\rm a}} f_j(q)\left\{\sum_{m=-\infty}^{+\infty}\exp\left(-im\frac{2\pi}{P_{\rm a}}u_z^j\right)\sum_{n=-\infty}^{+\infty}J_n(q_r r_j) \times \exp\left[-in(\psi_q - \varphi_0^j + \pi/2)\right]\mathrm{sinc}\left[L\frac{\Delta q_z(m,n)}{2\pi}\right]\right\}, \quad (13)$$

where $q_z(m, n)$ is defined as $2\pi[(n/P) + (m/P_{\rm a})]$ and $\Delta q_z(m, n)$ as $q_z - q_z(m, n)$, the sinc function is defined as $\mathrm{sinc}(x) = \sin(\pi x)/\pi x$, and J_n are Bessel functions of the first kind. Each helix has only one kind of element, meaning that this expression can not be used for nanowires made of random alloys. In the case of twisted nanowires, we always have $P \gg P_{\rm a}$, and thus around each m diffraction order we will have a set of n type diffraction orders that will vanish when moving along q_z away from the $n = 0$ helix diffraction order.

Since the helix pitch P is fixed by the torsion, the length L of the nanowire is not in general an integer number multiplied by P. Fig. 3 shows a three-dimensional representation of the diffraction from a single atomic helix with an arbitrary length equal to 5.5 periods ($L = 5.5P$) in the vicinity of $[q_r = 0, q_z = q_z(m, 0)]$. Because $P \gg P_{\rm a}$, the contributions of other values of m are neglected. A consequence is that the diffraction pattern of Fig. 3 is centrosymmetric with respect to $[q_r = 0, q_z = q_z(m, 0)]$. When the length L of the nanowire divided by the period P is not an integer, as in the case of Fig. 3, one can notice a dependence of the intensity on ψ_q. This dependence comes from the phase factor $\exp(-in\psi_q)$ in equation (13), which introduces a ψ_q-dependent interference between different helix diffraction orders.

On the other hand, when L is an integer number of periods, and still at the exact position of a helix diffraction order n, *i.e.* for $\Delta q_z(m, n) = 0$, the amplitudes of all the other helix diffraction orders (m, n) are equal to 0. Thus, if we neglect the contributions coming from other values of m (because

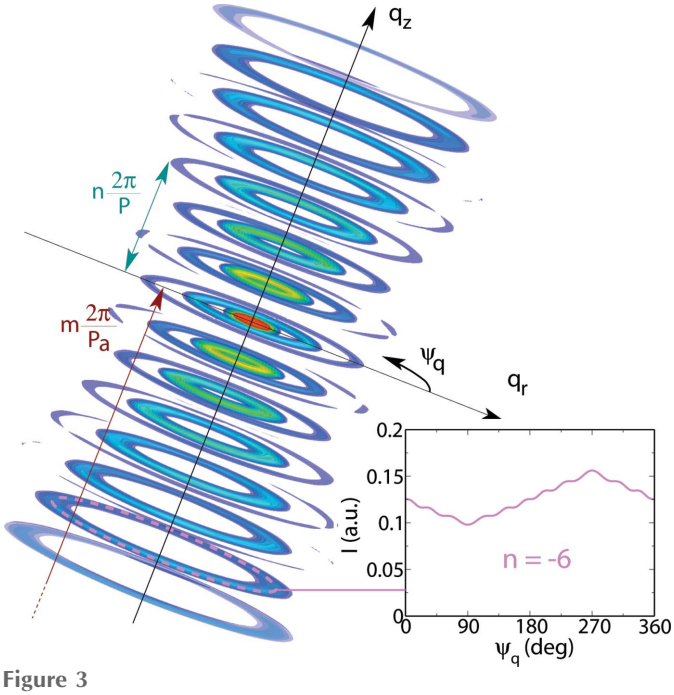

Figure 3
Three-dimensional representation of the calculated diffraction from a single helix of period P, composed of atoms that are regularly spaced and separated by a distance $P_{\rm a}$ along z, in the vicinity of $q_z = m2\pi/P_a$. The length of the helix is equal to 5.5 periods. The inset shows the ψ_q dependence of the intensity along the main ring of the $n = -6$ helix diffraction order.

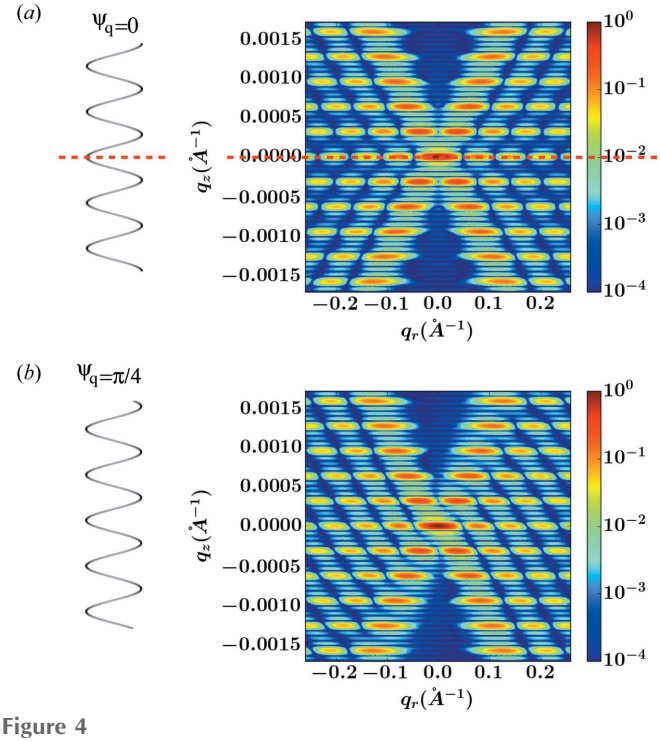

Figure 4
The ψ_q dependence of the diffraction demonstrated for two radial slices of the three-dimensional diffraction pattern of a five-period helix. On the left-hand side are shown projections of the helix in the direction perpendicular to the slices. (*a*) $\psi_q = 0$ and there is a mirror symmetry in the helix projection and in the diffraction pattern. The plane of symmetry is indicated by a red dashed line. (*b*) $\psi_q = \pi/4$ and the diffraction pattern is only centrosymmetric. The centre of symmetry is at the maximum of intensity in the diffraction pattern. Normalized intensities are represented on a logarithmic colour scale.

$P_a \ll P$), there is no ψ_q dependence of the intensity. However, even in the case where L/P is an integer, if we move away from the exact position $q_z = q_z(m, n)$ to positions between the rings of Fig. 3, a dependence on ψ_q appears. This is illustrated in Fig. 4, which shows two radial slices of the diffraction from a five-period helix calculated for two different values of ψ_q. According to the Fourier-slice theorem (see Appendix A), each radial slice (ψ_q constant) in the three-dimensional diffraction pattern is the two-dimensional Fourier transform of the helix projection along the axis perpendicular to the plane of the slice. To illustrate this point, two different projections are represented in Figs. 4(*a*) and 4(*b*). In the case of Fig. 4(*a*) the projection has a mirror symmetry which, in agreement with the Curie principle, can also be found in the corresponding diffraction slice on the right, in addition to the centrosymmetry. In the case of Fig. 4(*b*) there is no particular symmetry in the projection and the diffraction slice is only centrosymmetric.

3.2. Diffraction from a set of regularly spaced equivalent helices

Using the expression in equation (13) of the amplitude diffracted by a single helix, we may now calculate the amplitude diffracted by a set of k equivalent helices containing the same element, having the same radius r_0 and having the same chirality, as illustrated in Fig. 5(*b*) for $k = 4$. These helices have equally spaced angular positions $\varphi_0^j = j2\pi/k$ and a common displacement u_z^j taken to be equal to 0. For the purpose of this calculation we consider the amplitude in the vicinity of ($q_r = 0$, $\varphi_q = 0$, $q_z = m_0 2\pi/P_a$),

$$\mathcal{A}_k^{m_0}(\mathbf{q}) = F(q) \sum_{n=-\infty}^{+\infty} \left[J_n(q_r r_0)\; G_{n,m_0}(\mathbf{q}) \sum_{j=1}^{k} \exp\left(in\varphi_0^j\right) \right], \quad (14)$$

where

$$G_{n,m_0}(\mathbf{q}) = \exp\left[-in(\psi_q + \pi/2)\right] \operatorname{sinc}\left[L\frac{\Delta q_z(m_0, n)}{2\pi} \right] \quad (15)$$

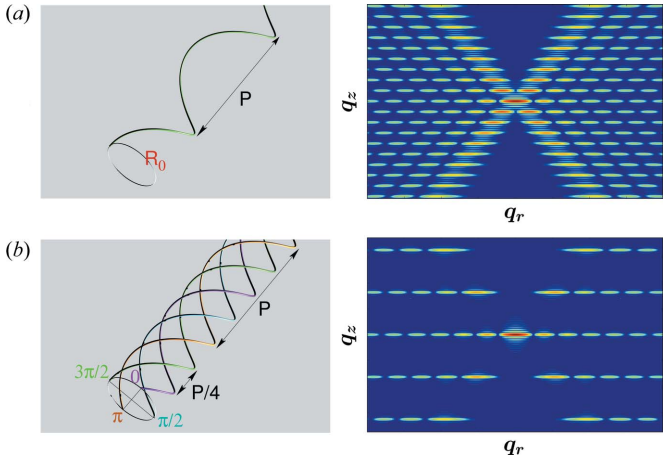

Figure 5
Diffraction from (*a*) a single helix and (*b*) four regularly spaced helices. In this latter case the period in real space is four times smaller than in the former case, and four times larger in reciprocal space.

and

$$F(q) = \frac{f_e L}{P_a} f_0(q). \quad (16)$$

As

$$\sum_{j=1}^{k} \exp\left(in\varphi_0^j\right) = \frac{\sin \pi n}{\sin \pi n/k} \exp\left[in\pi(1 - 1/k)\right] = \begin{cases} k & \text{if } n \equiv 0 \bmod k \\ 0 & \text{otherwise} \end{cases} \quad (17)$$

we finally obtain

$$\mathcal{A}_k^{m_0}(\mathbf{q}) = kF(q) \sum_{n=-\infty}^{+\infty} J_{nk}(q_r r_0)\; G_{nk,m_0}(\mathbf{q}). \quad (18)$$

Equation (18) shows that only one helix order every k will be visible. This important extinction rule is illustrated in Fig. 5, where the case of a single helix ($k = 1$) is compared with a set of four helices ($k = 4$). As shown in Fig. 5, the diffraction pattern of k equivalent helices can be viewed as the diffraction pattern of a single structure having a shorter period equal to P/k. In other words, increasing the number of equivalent helices will move diffraction features related to the helicity away from the crystal reciprocal-lattice points. Finally, note that, as this extinction rule relies on a regular spacing and constant displacement between the helices, it will be modified if their displacements u_z^j along the nanowire axis are not the same.

4. Results

In this section we focus on ⟨011⟩-oriented f.c.c. metallic nanowires where both the elastic anisotropy of the metal and the shape anisotropy of the cross section can interplay. Two significant asymptotic cases are detailed in the following. (i) The first situation, considered in §4.1, corresponds to the diffraction of a twisted ⟨011⟩ nanowire where the cross section is circular. Thus, the radial positions of the helices in a cross section are contained in a disc (shape isotropy) but their positions along z obey the twofold warping displacement field induced by the elastic anisotropy and expressed in equation (2). (ii) The second situation, discussed in §4.2, corresponds to the particular case of a pure shape-anisotropy effect where the warping is null. This equilibrium state under torsion is achieved by considering a twisted nanowire having a particular elliptic cross section (shape anisotropy) and an elastic anisotropy whose combined effects on the warp cancel each other, as described in Fig. 2.

Concerning the diffraction patterns shown in this section, let us mention that the intensity is divided by $f(q)^2$, meaning that the slow variations in the atomic scattering factor with q are not taken into account. As the atomic scattering factor also depends on energy, in a way which depends on the atomic element, this normalization also makes possible the comparison of diffraction patterns obtained from different materials. The simulated diffraction patterns are obtained around the 044 reflection, which is far enough from the reciprocal-space

origin to be sensitive to displacements, but not too far to be measured in the energy range usually used at synchrotrons and in laboratories for diffraction studies.

4.1. Effect of elastic anisotropy on diffraction through the warping displacement

If we consider a ⟨011⟩ nanowire with a circular cross section, the warping displacement u_z^j of a column j of polar coordinates (r_j, φ_0^j) can be written [from equation (2)]

$$u_z^j = u_z(r_j)\cos 2\varphi_0^j \quad \text{with} \quad u_z(r) = r^2\frac{\alpha}{2}\frac{1-A_z}{1+A_z}, \tag{19}$$

where α is the nanowire twist. The reference for the φ_0^j angle is taken at $-\pi/4$ of the [100] direction. Supposing that $P \gg P_a$, the amplitude diffracted by this helical atomic column in the vicinity of $(q_r = 0, q_z = m2\pi/P_a)$ is given by equation (13):

$$\mathcal{A}_j(\mathbf{q}) = \frac{f_e L}{P_a} f_j(q)\left\{\exp\left[-im\frac{2\pi}{P_a}u_z(r_j)\cos 2\varphi_0^j\right]\sum_{n=-\infty}^{+\infty} J_n(q_r r_j) \times \exp\left[-in(\psi_q - \varphi_0^j + \pi/2)\right]\operatorname{sinc}\left[L\frac{\Delta q_z(m,n)}{2\pi}\right]\right\}. \tag{20}$$

If the nanowire radius is not too small we can consider that the number of columns in a ring of radius r and width dr, and in an angular sector dφ, is $\rho_s r\,\mathrm{d}r\,\mathrm{d}\varphi$, where ρ_s is a column density by unit of cross section surface. The amplitude diffracted by this ring is

$$\mathrm{d}\mathcal{A}_r(\mathbf{q}) = \frac{f_e L}{P_a} f_j(q)\rho_s 2\pi r\,\mathrm{d}r\left\{\sum_{n=-\infty}^{+\infty}\mathcal{I}_n(r)J_n(q_r r) \times \exp\left[-in(\psi_q + \pi/2)\right]\operatorname{sinc}\left[L\frac{\Delta q_z(m,n)}{2\pi}\right]\right\}, \tag{21}$$

with

$$\mathcal{I}_n(r) = \int_{\varphi_0=0}^{2\pi}\exp\left[-im\frac{2\pi}{P_a}u_z(r)\cos 2\varphi_0\right]\exp(in\varphi_0)\,\mathrm{d}\varphi_0. \tag{22}$$

The calculation of $\mathcal{I}_n(r)$ is given in Appendix *B* and we have

$$\mathrm{d}\mathcal{A}_r(\mathbf{q}) = \frac{f_e L}{P_a} f_j(q)\rho_s 4\pi^2 r\,\mathrm{d}r\left\{\sum_{k=-\infty}^{+\infty}\exp(i3k\pi/2)J_k\left[m\frac{2\pi}{P_a}u_z(r)\right] \times J_{2k}(q_r r)\exp\left[-i2k(\psi_q + \pi/2)\right] \times \operatorname{sinc}\left[L\frac{\Delta q_z(m,2k)}{2\pi}\right]\right\}. \tag{23}$$

Fig. 6 shows the warp-dependent coefficient $J_k[m(2\pi/P_a)\,u_z(r)]$ which modulates the even helix diffraction orders $2k$. Considering the expression of u_z in equation (19), an initial conclusion is that the visibility of the high helix diffraction orders will be enhanced for higher values of r, α and A_z. In particular, for an isotropic crystal where $A_z = 1$, no helix-specific diffraction order (*i.e.* greater than 0) will be visible.

The amplitude diffracted by the twisted nanowire is obtained by integration with respect to r of d$\mathcal{A}_r(\mathbf{q})$, given by equation (23). Because d$\mathcal{A}_r(\mathbf{q})$ is proportional to r, the major contribution will come from the parts of the nanowire far from the axis which were already predicted to give the major contribution to the higher helix diffraction orders. Fig. 7 compares the diffraction patterns obtained for twisted nanowires of metals with different asymmetry factors A_z, including a virtual isotropic metal, for which there is no evidence of helix diffraction. In the case of Al, only the first-order $(-1, +1)$ helix diffraction orders appear, whereas in the case of Cu the X-shaped pattern, commonly associated with diffraction by helices, is clearly visible. The simulations of Fig. 7 are in good agreement with the discussion of Fig. 6, namely the dependence of the J_k terms on A_z.

An additional comment can be made for the case of an isotropic crystal. The result obtained in Fig. 7 for $A_z = 1$ corresponds well with what we might expect from the extinction rule described in §3.2 for k equivalent helices. Since there is no warp for $A_z = 1$, all helices contained in a ring of radius r are equivalent and statistically regularly spaced. Besides, the main contribution to diffraction comes from large rings and therefore from large numbers of equivalent helices. This explains the large number of extinguished helix orders observed in Fig. 7 for $A_z = 1$ (see supporting information).

A question that may arise concerns the validity of this continuous model for nanowires which are actually composed of a discrete number of helices. A comparison was made using MS simulations to obtain the helix warping displacements in a Cu nanowire of 10 nm radius. The results, reported in the supporting information, show very good agreement between a discrete summation of the helix amplitudes and the diffracted amplitude given by the continuous model.

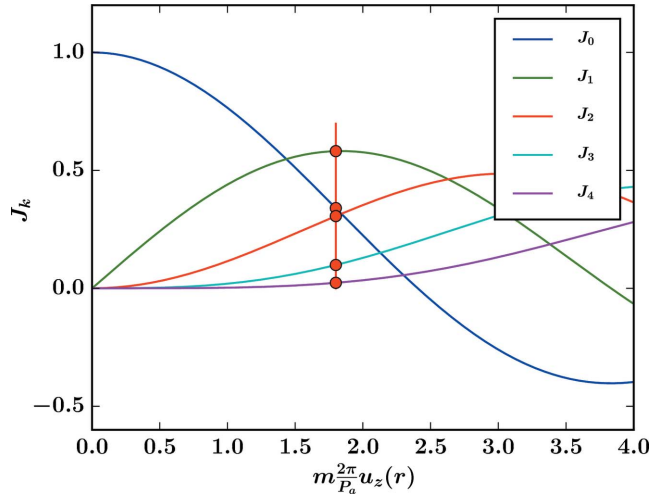

Figure 6
Warp-dependent helix diffraction order coefficients as a function of the warp radial part $m(2\pi/P_a)u_z(r)$ (solid lines). Red circles correspond to a particular value of $m(2\pi/P_a)u_z(r) = 1.8$.

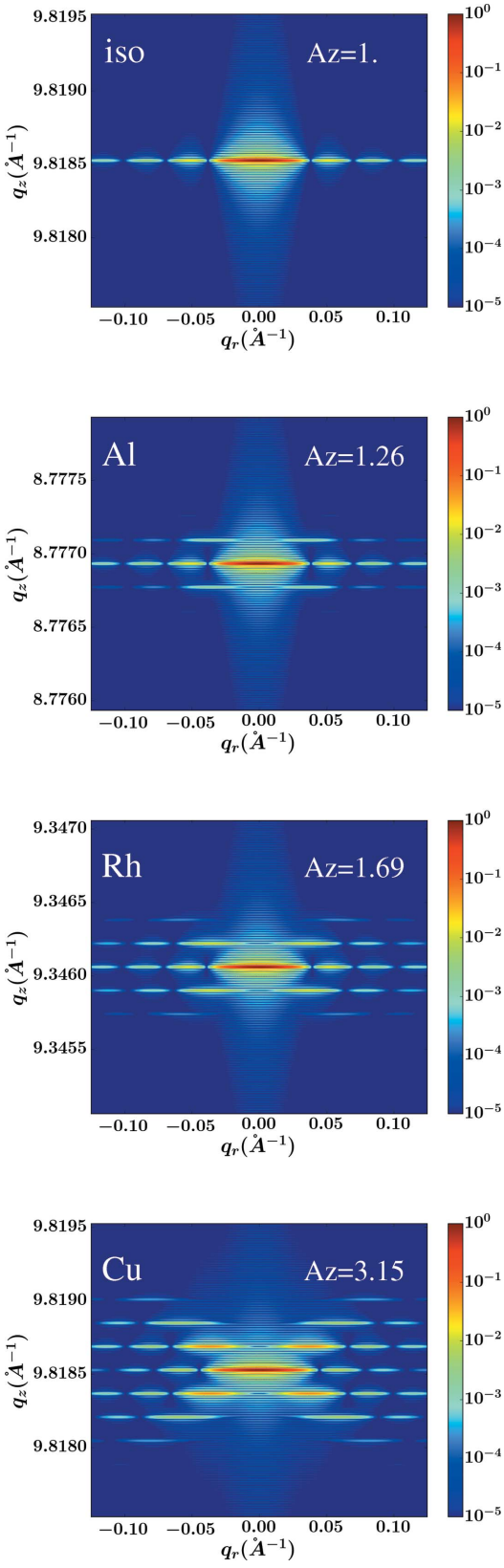

Figure 7
Comparison of the simulated diffraction patterns $[|A(\mathbf{q})|^2/f_j(q)^2]$ around the 044 reflection for metals presenting different anisotropy factors A_z, including a virtual isotropic crystal ($A_z = 1$). The nanowire radius (10 nm), torsion (8×10^{-4} rad nm^{-1}) and length (5 periods) are identical for the three metals and the isotropic crystal. Normalized intensities are represented on a logarithmic colour scale.

4.2. Effect of shape anisotropy

In this section we calculate the amplitude diffracted by a twisted ⟨011⟩ nanowire with an elliptic cross section for which the warping displacement is equal to zero [with $a/b = (A_z)^{1/2}$ in equation (2) and Fig. 2]. In this case we have a pure shape anisotropy, although this anisotropy is related to the elastic anisotropy. As in the case of §4.1, a continuous model is used. We replace in equation (21) the integral $\mathcal{I}_n(r)$ with the integral $\mathcal{I}'_n(r)$,

$$\mathcal{I}'_n(r) = [1 + \exp(in\pi)] \int_{\varphi_0=-\varphi_0(r)}^{\varphi_0(r)} \exp(in\varphi_0)\, \mathrm{d}\varphi_0$$
$$= 2[1 + \exp(in\pi)] \frac{\sin[n\varphi_0(r)]}{n}, \qquad (24)$$

where

$$\varphi_0(r) = \begin{cases} \pi/2 & \text{for } r \le b, \\ 0 & \text{for } r \ge a, \\ \arccos\left[\left(\dfrac{1 - b^2/r^2}{1 - b^2/a^2}\right)^{1/2}\right] & \text{for } b < r < a. \end{cases} \qquad (25)$$

Here, the phase factor related to the u_z displacement has disappeared because the displacements for all the atomic columns are identical and can be taken equal to zero. Also, owing to the elliptic shape (see Fig. 8), the interval of integration [0:2π] of $\mathcal{I}_n(r)$ in equation (22) is replaced by the r-dependent interval $[-\varphi_0(r):\varphi_0(r)]$ for the integral $\mathcal{I}'_n(r)$ in equation (24). The amplitude diffracted by the part of the twisted nanowire between r and $r + \mathrm{d}r$ is

$$\mathrm{d}\mathcal{A}_r(\mathbf{q}) = \frac{2f_e L}{P_a} f_j(q)\rho_s 2\pi r\, \mathrm{d}r \left\{ \sum_{k=-\infty}^{+\infty} \exp(ik\pi/2) \frac{\sin[2k\varphi_0(r)]}{k} \right.$$
$$\times J_{2k}(q_r r) \exp\left[-i2k(\psi_q + \pi/2)\right]$$
$$\left. \times \operatorname{sinc}\left[L \frac{\Delta q_z(m, 2k)}{2\pi}\right] \right\}, \qquad (26)$$

where n is replaced by $2k$ because the integral $\mathcal{I}'_n(r)$ in equation (24) is different from zero for even values of n.

The total diffracted amplitude is obtained by integration with respect to r over the interval [0:a]. From equation (26) we can guess that the core of the nanowire for $r < b$ will only

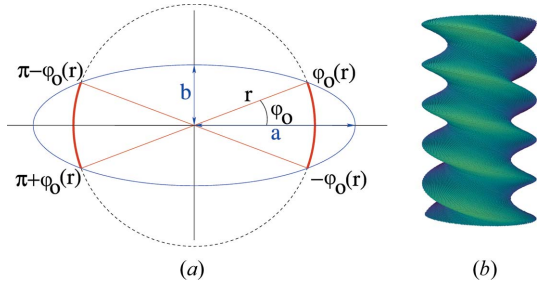

Figure 8
(*a*) The geometry of the elliptic nanowire cross section, showing the angular integration regions for columns the same radial distance r from the nanowire axis. (*b*) An example of a twisted elliptic nanowire.

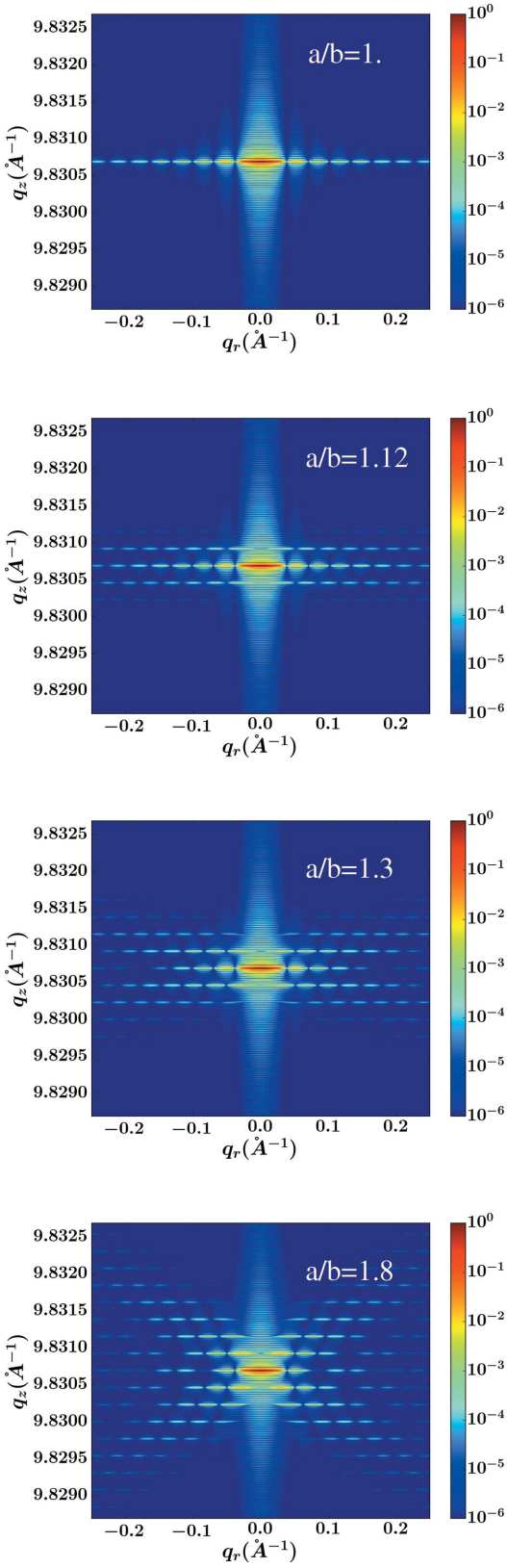

Figure 9
Comparison of the simulated diffraction patterns $[|A(\mathbf{q})|^2/f_j(q)^2]$ around the 044 reflection for elliptic nanowires presenting different eccentricities. The cross-section surface is kept constant and equal to the cross section of a circular 10 nm radius nanowire. The torsion is fixed at 1.15×10^{-3} rad nm^{-1} and the nanowires have a length of 5 periods. Normalized intensities are represented on a logarithmic colour scale.

contribute to the helix 0 order ($n = 2k = 0$), as was seen in Fig. 7 for the isotropic case $A_z = 1$. It can also be expected from equation (26) that a large eccentricity of the ellipse will give rise to higher helix orders in the diffraction pattern. Fig. 9 confirms this latter point. The more asymmetric the shape of the elliptic cross section, the more visible are the helix diffraction orders.

4.3. Discussion

The results shown above in §4.1 and §4.2 use a continuous integration which works very well for nanowires with a radius in the range of 10 nm (see the comparison with the discrete atomistic approach in the supporting information). The tendency predicted by our model is, however, still valid, although less strictly, for nanowires with a very small radius such as the one depicted in Fig. 1. This is demonstrated in Fig. 10 by performing MS simulations of a 1 nm radius twisted ⟨011⟩ nanowire with a circular cross section. Fig. 10(*b*) shows the diffraction pattern calculated from the relaxed atomic positions, while Fig. 10(*a*) corresponds to the diffraction pattern before relaxation when the torsion warping is still equal to zero. The fact that a few helix diffraction orders are visible in Fig. 10(*a*) can be attributed to the fact that the cross section for such a low radius is not perfectly circular and appears as slightly anisotropic. It is also clear that the effect of the torsion warping, related to the elastic anisotropy, is still very marked (Fig. 10*b*).

Another point is that shape or elastic anisotropy in the plane of the cross section is only a necessary condition to observe helix-related features in twisted-nanowire diffraction patterns. As a consequence, a twisted ⟨001⟩ Cu nanowire with a circular cross section that is known to behave isotropically under torsion [the warp is null according to equation (1)] should not reveal its helicity in the diffraction pattern. This is well verified in Fig. 11(*a*), where the X-shaped pattern is not observed in the case of this ⟨001⟩ nanowire.

For the sake of clarity, we have chosen to detail cases presenting pure effects of elastic anisotropy or pure effects of shape anisotropy. In real nanowires these two effects might be combined. For example, ⟨011⟩ Cu nanowires present a lateral surface with {001} and {111} facets, giving to their cross section a pseudo-hexagonal shape. Fig. 11(*b*) shows the diffraction pattern for such a nanowire, with a clear signature of its helicity.

Concerning the question of the possibility of experimental measurement of the effects shown in this publication, the main problem might not be related to the measurement of nanowires of very small radius. Indeed, measurements have already been carried out on nanowires with radii down to 25 nm (Labat, 2018). This is just above the 10 nm value used for most of the simulations in this publication and we can expect the limit to be lowered in the near future using recent or upgraded third-generation synchrotrons or X-ray free-electron lasers. The main difficulties might be the manipulation of such small objects and the realization of torsion experiments.

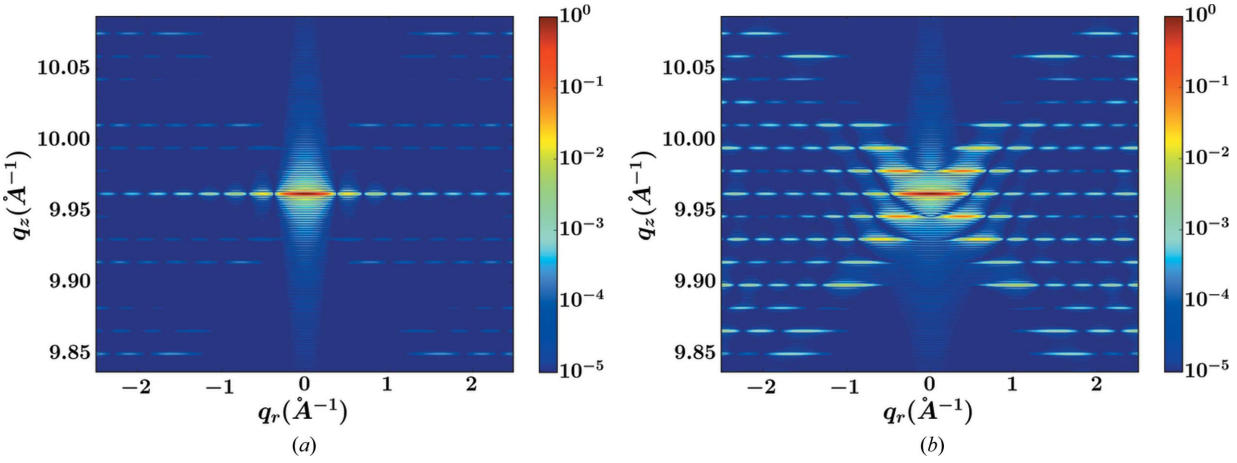

Figure 10
Diffraction around the 044 reflection from a 1 nm radius twisted nanowire with a circular cross section from MS simulations. (*a*) The atomic positions are partially relaxed and the warp along z is maintained to be equal to 0. (*b*) The atomic positions are fully relaxed, including the warp effect. The torsion is equal to 8×10^{-2} rad nm^{-1}. Normalized intensities are represented on a logarithmic colour scale.

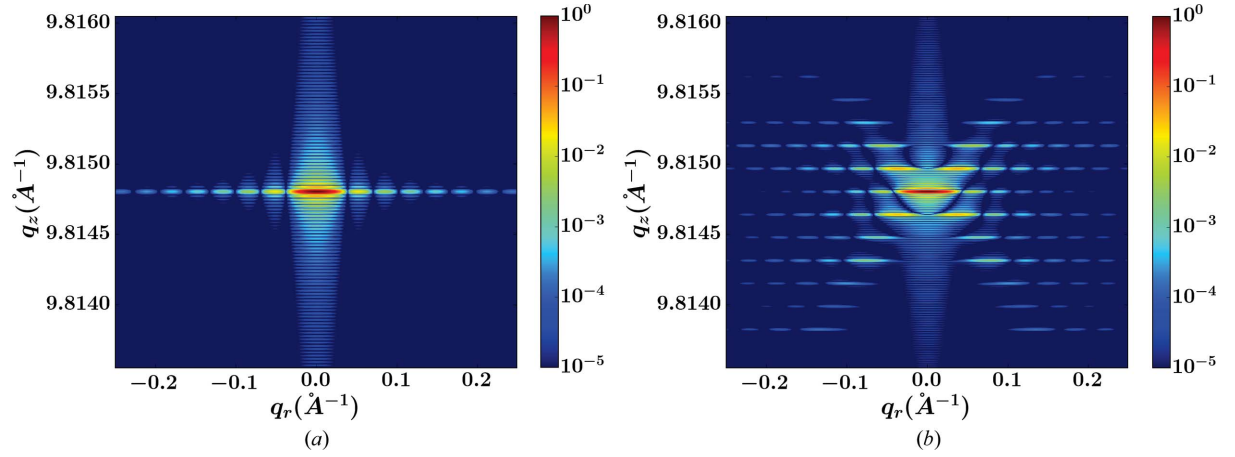

Figure 11
(*a*) Diffraction around the 004 reflection from an ⟨001⟩-oriented 10 nm twisted nanowire. The torsion is 1.15×10^{-3} rad nm^{-1}. (*b*) Diffraction around the 044 reflection from an ⟨011⟩-oriented nanowire with a nearly hexagonal cross section. The cross-section surface is the same as a circular nanowire of radius 10 nm and the torsion is 8×10^{-4} rad nm^{-1}. The relaxed positions of the atomic helices are given by the MS simulations. Normalized intensities are represented on a logarithmic colour scale.

Finally, note that helicity on a very different scale may exist in a nanowire that contains an axial screw dislocation. In this case, the helix pitch P is the Burgers vector modulus of the screw dislocation and the atomic period P_a becomes very small when r increases. This case is discussed in Appendix *C*. The two kinds of helicity may also combine in a free nanowire with an axial screw dislocation, as the dislocation is stabilized by the Mann–Eshelby twist which cancels the torque created by the dislocation (Eshelby, 1953; Mann, 1949; Roussel & Gailhanou, 2015).

5. Conclusions

In this study, using the kinematic diffraction theory developed in the past for diffraction from a helix (CCV theory), we have derived expressions for the diffraction from twisted nanowires.

A first expression is obtained for the case of a nanowire with a circular cross section. It is shown that the signature of helicity in the diffraction pattern (*i.e.* the famous X-shaped diffraction pattern observed by Franklin and Gosling for DNA) is revealed when there is a torsion-induced warping displacement along the wire axis. According to elasticity theory, this latter depends on the crystal anisotropy and the wire orientation. For a ⟨011⟩ Cu nanowire, the warping displacement of the atomic helices forming the twisted nanowire has a twofold symmetry. Helices that are all equivalent in a ring of the nanowire without warp are now found equivalent only two by two when displaced by the twofold warp. In this work, we have shown that this lowering of symmetry caused by the warp is responsible for the X-shaped pattern in the reciprocal-space map.

A second continuous model for diffraction is derived for twisted nanowires presenting an elliptic cross section but no torsion-warping displacement. From this particular case, we conclude that pure anisotropic shape effects can also reveal the helicity of the twisted nanowire. More generally, we

conclude that elastic or shape anisotropy with respect to the wire orientation is a necessary condition for the presence of helicity features in the diffraction patterns of a perfect twisted crystalline nanowire. This rule remains valid even for very low radius nanowires according to our MS simulations.

Finally, we report the possibility of another source of helicity on a very different scale due to the presence of an axial screw dislocation in the nanowire.

APPENDIX *A*
Fourier-slice theorem

If $F(q_x, q_y, q_z)$ is the Fourier transform of $\rho(x, y, z)$, then

$$\begin{aligned} F(q_x, 0, q_z) &= \iiint \rho(x, y, z) \exp\left[-i(q_x x + q_z z)\right] \mathrm{d}x\, \mathrm{d}y\, \mathrm{d}z \\ &= \iint \Big[\int \rho(x, y, z)\, \mathrm{d}y\Big] \exp\left[-i(q_x x + q_z z)\right] \mathrm{d}x\, \mathrm{d}z. \end{aligned} \tag{27}$$

Consequently, the two-dimensional slice with $q_y = 0$ of the three-dimensional Fourier transform of $\rho(x, y, z)$ is equal to the two-dimensional Fourier transform of the projection of $\rho(x, y, z)$ along y.

APPENDIX *B*
Calculation of $\mathcal{I}_n(r)$

$$\mathcal{I}_n^m(r) = \int_{\varphi_0=0}^{2\pi} \exp\left[-im\frac{2\pi}{P_\mathrm{a}} u_z(r)\cos 2\varphi_0\right] \exp\left(in\varphi_0\right) \mathrm{d}\varphi_0. \tag{28}$$

We write $\varphi_0' = 2\varphi_0$:

$$\begin{aligned} \mathcal{I}_n^m(r) &= \frac{1}{2} \int_{\varphi_0'=0}^{4\pi} \exp\left[-im\frac{2\pi}{P_\mathrm{a}} u_z(r)\cos\varphi_0'\right] \exp\left(in\varphi_0'/2\right) \mathrm{d}\varphi_0' \\ &= \frac{1}{2}\left[1 + \exp\left(in\pi\right)\right] \int_{\varphi_0'=0}^{2\pi} \exp\left[-im\frac{2\pi}{P_\mathrm{a}} u_z(r)\cos\varphi_0'\right] \\ &\quad \times \exp\left(in\varphi_0'/2\right) \mathrm{d}\varphi_0'. \end{aligned} \tag{29}$$

For $n = 2k + 1$ where k is an integer, $\mathcal{I}_n^m(r) = 0$, and for $n = 2k$

$$\begin{aligned} \mathcal{I}_n^m(r) &= \int_{\varphi_0'=0}^{2\pi} \exp\left[-im\frac{2\pi}{P_\mathrm{a}} u_z(r)\cos\varphi_0'\right] \exp\left(ik\varphi_0'\right) \mathrm{d}\varphi_0' \\ &= 2\pi \exp\left(i3k\pi/2\right) J_k\left[m\frac{2\pi}{P_\mathrm{a}} u_z(r)\right]. \end{aligned} \tag{30}$$

This last expression is obtained using an integral expression of the Bessel function of the first kind (Jahnke & Embde, 1945),

$$J_k(z) = \frac{i^{-k}}{2\pi} \int_0^{2\pi} \exp\left(iz\cos\varphi\right) \exp\left(ik\varphi\right) \mathrm{d}\varphi. \tag{31}$$

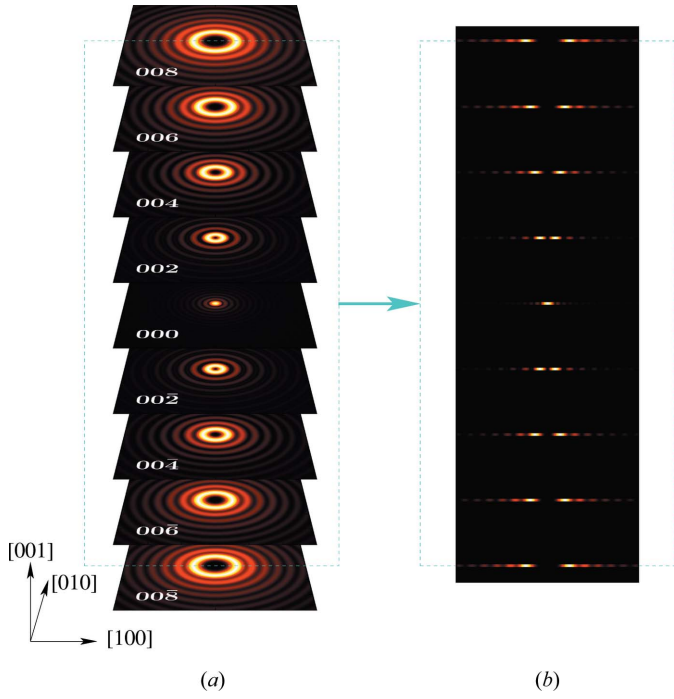

Figure 12
Diffraction from a ⟨001⟩ nanowire with an axial screw dislocation. (*a*) A three-dimensional view built from simulations of $002n$ diffraction patterns, with n varying from −4 to 4. (*b*) An axial cross section of the three-dimensional view, showing the familiar X-shaped pattern related to diffraction from helices.

APPENDIX *C*
A nanowire with an axial screw dislocation viewed as a helical system

In this appendix, we calculate the amplitude diffracted by a cylindrical rod with an axial screw dislocation by considering the rod as a set of helices j of different radii with the same pitch equal to the Burgers vector, the same angular position φ_0^j and the same position along z ($u_z^j = 0$). We compare the result of this calculation with that derived by Wilson (1952), and we show that the helical character of the screw dislocation is very clear in the diffraction patterns.

If h is the projected distance between nearest-neighbour atoms in the cross-section plane, the atomic periodicity P_a along z for a helix of radius r and width $\mathrm{d}r$ can be written as

$$P_\mathrm{a} = h\frac{b}{2\pi r}, \tag{32}$$

where b is the modulus of the screw-dislocation Burgers vector. For increasing values of r, P_a becomes very small, which allows us to consider only the $m = 0$ term in the sum of equation (13) for the calculation of the amplitude diffracted by the helix $(r, \mathrm{d}r)$. Moreover, if we calculate only the amplitude diffracted at the exact position of order n (the sinc function is taken to be equal to 1), we get

$$\mathrm{d}\mathcal{A}_n \propto \frac{2\pi r}{bh}(-i)^n \exp\left(-in\psi_q\right) J_n(q_r r)\, \mathrm{d}r. \tag{33}$$

By integration with respect to r we obtain the amplitude diffracted at order n by the nanowire:

$$\mathcal{A}_n \propto \frac{2\pi(-i)^n \exp(-in\psi_q)}{bh} \int_0^R J_n(q_r r) r \, \mathrm{d}r. \qquad (34)$$

This expression is equivalent to that obtained by Wilson (1952), except that the phase factor $\exp(-in\psi_q)$ was omitted by Wilson at some point in his calculation by taking $\psi_q = 0$. Here again the major contribution comes from the larger values of r. Fig. 12 shows the calculated diffraction orders for a nanowire with an axial screw dislocation from equation (34). Clearly, we can recognize the specific helix diffraction pattern, in three dimensions as in Fig. 3 or in two dimensions as in the famous Franklin and Gosling DNA diffraction pattern (Franklin & Gosling, 1953).

Acknowledgements

The authors thank Stephane Labat for helpful discussions.

References

Amara, M.-S. (2014). PhD thesis, Université Paris-Sud – Paris XI, France.
Barlow, D. & Thornton, J. (1988). *J. Mol. Biol.* **201**, 601–619.
Caspar, D. (1956). *Nature*, **177**, 928.
Cochran, W., Crick, F. H. & Vand, V. (1952). *Acta Cryst.* **5**, 581–586.
Davtyan, A., Lehmann, S., Kriegner, D., Zamani, R. R., Dick, K. A., Bahrami, D., Al-Hassan, A., Leake, S. J., Pietsch, U. & Holý, V. (2017). *J. Synchrotron Rad.* **24**, 981–990.
Diaz, R., William, J. R. & Stokes, D. L. (2010). *Cryo-EM*, Part B, *3-D Reconstruction*, edited by G. J. Jensen, *Methods in Enzymology*, Vol. 482, pp. 131–165. New York: Academic Press.
Eshelby, J. (1953). *J. Appl. Phys.* **24**, 176–179.
Favre-Nicolin, V., Mastropietro, F., Eymery, J., Camacho, D., Niquet, Y. M., Borg, B. M., Messing, M. E., Wernersson, L.-E., Algra, R. E., Bakkers, E. P. A. M., Metzger, T. H., Harder, R. & Robinson, I. K. (2010). *New J. Phys.* **12**, 035013.
Franklin, R. (1956). *Nature*, **177**, 928–930.
Franklin, R. & Gosling, R. (1953). *Nature*, **171**, 740–741.
Gailhanou, M. & Roussel, J.-M. (2013). *Phys. Rev. B*, **88**, 224101.
Higgins, T. J. (1942). *Am. J. Phys.* **10**, 248–259.
Jahnke, E. & Embde, F. (1945). *Tables of Functions with Formulae and Curves*, 4th ed. New York: Dover Publications.
Labat, S. (2018). Personal communication.
Labat, S., Richard, M.-I., Dupraz, M., Gailhanou, M., Beutier, G., Verdier, M., Mastropietro, F., Cornelius, T. W., Schülli, T. U., Eymery, J. & Thomas, O. (2015). *ACS Nano*, **9**, 9210–9216.
Lambin, P. & Lucas, A. A. (1997). *Phys. Rev. B*, **56**, 3571–3574.
Lekhnitskii, S. (1981). *Theory of Elasticity of an Anisotropic Body*. Moscow: MIR.
Lucas, A. A. & Lambin, P. (2005). *Rep. Prog. Phys.* **68**, 1181–1249.
Mann, E. H. (1949). *Proc. R. Soc. London Ser. A*, **199**, 376–394.
Maurer, F., Brötz, J., Karim, S., Toimil Molares, M. E., Trautmann, C. & Fuess, H. (2007). *Nanotechnology*, **18**, 135709.
Pauling, L., Corey, R. & Branson, H. (1951). *Proc. Natl Acad. Sci. USA*, **37**, 205–211.
Prodanovic, M., Irving, T. C. & Mijailovich, S. M. (2016). *J. Appl. Cryst.* **49**, 784–797.
Ranganathan, S. I. & Ostoja-Starzewski, M. (2008). *Phys. Rev. Lett.* **101**, 055504.
Roussel, J.-M. & Gailhanou, M. (2015). *Phys. Rev. Lett.* **115**, 075503.
Watson, J. & Crick, F. (1953). *Nature*, **171**, 737–738.
Weinberger, C. R. & Cai, W. (2010). *J. Mech. Phys. Solids*, **58**, 1011–1025.
Wilkins, M., Stokes, A. R. & Wilson, H. (1953). *Nature*, **171**, 738–740.
Wilson, A. J. C. (1952). *Acta Cryst.* **5**, 318–322.